Longitudinal Trim Analysis for Aircraft Icing from the SENS4ICE European Flight Test Campaign

Christoph Deiler*, Falk Sachs†
DLR (German Aerospace Center), Braunschweig, 38108, Germany

Icing has various impacts on the aircraft flight characteristics. There are several well-known general effects, like the increase of drag due to ice accretion on the airframe or the decrease of lift as well as a highly nonlinear lift behavior during flow separation and reduced stall onset angle of attack caused by ice formation on the lifting surfaces. In addition, icing on the tailplane changes the longitudinal trim characteristics and might lead to premature tailplane stall. To further investigate the longitudinal trim effect of icing caused by different icing conditions, a longitudinal trim analysis was performed based on flight test data gathered during the SENS4ICE European flight test campaign. The analysis focused on the different effects of icing caused by atmospheric conditions with different water droplet size. In this campaign also and especially conditions with supercooled large droplets, which are known to have even more hazardous effects on aircraft flight characteristics, were identified by meteorologists and intentionally intruded by the especially equipped research aircraft. The trimmed aircraft's elevator deflection and total pitch coefficient were analyzed for flight data sets related to different atmospheric conditions encountered during the different flights and compared to the clean (ice-free) aircraft reference flight data. Data were clustered for the certification icing envelopes (appendix C and appendix O), knowing that the ice formations caused are not uniform. Nevertheless, only small deviations from the clean aircraft elevator trim curves are noticeable for both icing data sets, being in line with the pilots' reports after the flights. However, the pitch moment curves show an obvious change of gradient (with angle of attack) for all icing cases.

Nomenclature

a_x, a_z	=	acceleration in x and z direction m/s^2
C_D	=	drag coefficient
C_{D0}	=	drag coefficient at zero lift
C_L	=	lift coefficient
C_{L0}	=	lift coefficient at zero angle of attack
$C_{L\alpha}$	=	lift coefficient slope
C_m	=	pitching moment coefficient
$C_{m\alpha}$	=	pitching moment coefficient slope
$\bar{c}$	=	mean aerodynamic chord, m
D	=	drag force, N
F	=	force, N
I_{xx}, I_{yy}, I_{xz}	=	moments and product of inertia, Nm^2
k_2	=	drag coefficient factor
L	=	lift force, N
M	=	pitching moment, Nm
m_{AC}	=	aircraft mass, kg
P	=	model parameter
$\mathcal{P}$	=	percentile/ quantile
p, q, r	=	rotational velocities, rad/s
$\overline{q}$	=	dynamic pressure, Pa

*Scientific Advisor, Institute of Flight Systems, Lilienthalplatz 7, Braunschweig, 38108, Germany, AIAA Senior Member
†Research Engineer, Institute of Flight Systems, Lilienthalplatz 7, Braunschweig, 38108, Germany

S_{Wing} = reference wing surface area, m^2
T = engine thrust force, N
X, Z = body-fixed forces, N
z = body-fixed vertical coordinate, m

α = angle of attack, rad
η = elevator deflection, rad

Subscripts

aero = aerodynamic
CG = center of gravity
meas = derived from flight data
RP = reference point
X, Z = body-fixed directions,

Acronyms

ATR = Avions de Transport Régional
CER = Contrôle Essais Réception
IID = Indirect Ice Detection
IPS = Ice Protection System
SENS4ICE = SENSors and certifiable hybrid architectures for safer aviation in ICing Environment
SLD = Supercooled Large Droplets

I. Introduction

Icing can have hazardous effects on airplane performance characteristics and can be a limiting factor for the safe flight envelope. The change of the dynamic behavior and potential premature stall raise the need for pilot situational awareness and an adaption of control strategy. Different accidents worldwide have shown the criticality of icing related aircraft characteristics degradations, e.g., Refs. [1–4], especially when caused by supercooled large water droplets (SLD). Although in most cases the involved aircraft were equipped with state-of-the-art ice protection systems, the hazardous effects of SLD ice accretion can still lead to catastrophic events. These icing conditions can pose a high risk to the aircraft, crew and passengers. Specific detection and countermeasures are required to assure aircraft safety during flight. The certification of (modern) transport aircraft for flight into (known) icing conditions was mainly based on the certification requirements given in the so-called App. C to e.g., CS-25. But with the identified hazards to fixed-wing aircraft resulting from SLD, the certification requirements were extended by the new App. O including SLD ice in 2014. From now on, manufacturers must prove that a newly developed airplane is also safe for flight into the even more hazardous SLD icing conditions. For flight safety it is now mandatory to detect the presence of SLD icing early. Furthermore, monitoring the aircraft's remaining capabilities during prolonged flight in icing conditions would give relevant information to the pilots about the required adaption of operation, e.g., if the aerodynamics are significantly degraded there is an urgent need to enter air masses with sufficiently warm temperatures to melt ice accretions on the airframe. As a complicating fact, predicting the distinct change of aircraft characteristics caused by SLD ice formation is challenging and still topic of current aviation research.

Ice protection systems (IPS) on transport aircraft may require a significant amount of energy provided on board. Thermal ice protection systems of mainly commercial aircraft usually rely on bleed air, which reduces the engine effectiveness and increases fuel consumption. Using such a system preventively therefore has a direct impact on aircraft emissions and operation cost. Aircraft using other sources of energy beyond fossils may also be significantly affected by the amount of energy needed for anti-ice or de-ice systems. A more deliberate activation of the IPS can lead to more efficient but safe flight operations for which a reliable information about, e.g., the IPS effectiveness against the current icing encounter would be necessary. This information could be provided by suitable ice detection methods giving a hint on the presence of icing conditions, actual ice formation on the airframe and the effect of icing on the flight characteristics [5, 6]. Moreover, it would also open possibilities for the modification of existing systems by modulating the thermal power according to the current need, directly reducing the energy consumption and increasing the aircraft efficiency.

Fig. 1 Safire ATR 42-320 flight test bench (MSN 78): aircraft with all modification for the SENS4ICE European flight test campaign at Toulouse/Francazal airport; credit DLR/Safire.

The goal of the European Union Horizon 2020 Project "'SENSors and certifiable hybrid architectures for safer aviation in ICing Environment"' (SENS4ICE) project (2019-2024) was to provide a more comprehensive overview on the icing conditions, ice formation and aircraft degradation status including the aircraft's remaining capabilities (icing-related change in aircraft flight physics, i.e., degraded aircraft performance) [7–9]. Within SENS4ICE, the "indirect ice detection" (IID) was further developed and matured and was one important project pillar [6, 10–12]. It is a novel methodology and system for the on-board surveillance of aircraft flight performance used for ice detection purposes and was originally formulated and presented as a performance-based ice detection methodology, e.g., in Ref. [5], being already under patent protection in several countries [13]. It utilizes the effect of aircraft performance degradation due to ice accretion on the airframe resulting in a change of aerodynamics. The idea of the IID is not restricted to an application on large transport aircraft but can also enable a reliable ice detection for aircraft systems, such as small aerial vehicles, which currently have no ice detection or protection system, but operate in hazardous environments with very different icing conditions.

The SENS4ICE project contained two major icing flight test campaigns: the North America campaign using an Embraer Phenom 300 prototype aircraft and the European campaign with an ATR 42-320 (see Fig. 1) operated by Safire [8, 14]. Having flight test data available* subsequent analysis and evaluations can be made, which were not in the focus during the project period of SENS4ICE. For the evaluation of the IID, aircraft aerodynamic performance data has been investigated case-by-case in order to validate the indirect ice detection accuracy [6, 11, 12, 15]. But the analysis was mainly focused on the aircraft drag polar, which shows a significant increase of drag at given lift (see Fig. 2a), and for example the pitching moment was not from interest so far.

Nevertheless, it could be of interest to investigate the icing effects on the pitching moment as well, as there is an expectable degradation of longitudinal dynamics according to the scientific consensus on the effects of icing on aerodynamics. Scientific work on aircraft icing from the 1980s and 1990s already revealed the effects of different ice shapes or configurations on airfoils, wings and the overall aircraft. There is the general expectation, that an iced aircraft experiences an increase in pitching moment† (see Fig. 2b) and decrease in elevator effectiveness [16]. This leads in general to a more nose up pitch tendency of the iced aircraft. In more detail, the effect of large droplet icing shapes on a NACA 0012 airfoil was analyzed in Ref. [17]. In Ref. [18] a review of existing data, mainly published in Ref. [19] and Ref [20] from tests with NASA's DHC-6 Twin Otter aircraft, showed that for simulated moderate glaze ice cases a change of elevator effectiveness and longitudinal stability appear with an increase of pitching moment slope ($C_{m\alpha}$) of around 10 %. Comparable numbers are reported for the investigation of a NACA 23012 airfoil[21]. In addition, a reduction of the elevator effectiveness of more than 10 % for an "all aircraft iced" case was reported from natural icing flight test [19]. Note that all such aircraft ice cases could be similar to the icing configuration of the aircraft during the SENS4ICE flight tests. But it is also reported in Ref. [19] that the effect of icing on the pitching moment was strongly dependent on the thrust conditions present during the test: with high thrust respectively engine torque settings the effect was much stronger than for low engine torques. Wind tunnel tests with a Twin Otter model and artificial ice shapes generated with LEWICE 2.0 for a 22.5 min encounter showed "a slight reduction in longitudinal stability ($C_{m\alpha}$) in the pre-stall region". Wind tunnel with an iced 1/12-scale aircraft model of an S-3B Viking revealed comparable results [22].

*part of the data is publicly available at `https://safireplus.aeris-data.fr/`

†according to different sources, there is no clear tendency on the resulting pitching moment slope with angle of attack due to icing; hence, the given reduction of $C_{m\alpha}$ is mainly symbolic and a reproduction from the information given in Ref. [16]

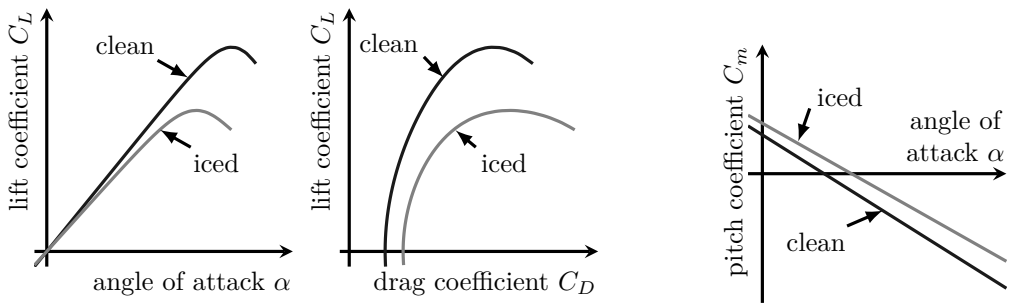

(a) lift and drag coefficient **(b) pitching moment coefficient**

Fig. 2 Expected influence of icing on aircraft aerodynamics; adapted from [16]

This paper contains evaluation results from the European fight test campaign conducted in April 2023 out of Toulouse (France) with a focus on the changes in aerodynamics, especially the aircraft pitch trim, for flight segments with steady atmospheric conditions. The flight test data used for the evaluation is presented section II, whereas the evaluation regarding the aerodynamic changes is part of section III. Finally, summary and conclusion are given in section IV.

II. Data Base from SENS4ICE Flight Test Campaign

The flights of the European flight test campaign in April 2023 were either performed as airways flights or (preferably) as CER flights. CER (Contrôle Essais Réception / Dedicated ATC for tests & acceptance) refers to specifically designated areas reserved for test aircraft. Flights in these areas were controlled by a dedicated controller, which provides a lot of flexibility for adjusting the flight plan. However, only a few CER zones were available for this flight campaign. If no suitable weather conditions were predicted for these regions, airways flights were conducted instead. These had basically no flexibility to make changes in the horizontal flight path. Fifteen scientific flights were performed within the European flight test campaign. Additionally, two observational flight have been conducted to identify possible issues with the aircraft flight test installation or to do special instrumentation tests. Hence, these flights were subsequently not evaluated.

For the presented longitudinal trim analysis, the flight data base with icing conditions was build from the remaining thirteen campaign flights. In total more than ten hours were spent in icing. During more than 2 hours of this time the aircraft flew in SLD (appendix O) conditions. Prior to the icing flight tests in April 2023, clean air flights had been conducted end of March to initially test the flight test instrumentation and reveal the clean aircraft's flight performance (c.f. [23]).

During the campaign, the flight test procedure was as follows: entering a icing cloud layer, preferably from below, flight through icing conditions, measuring the atmospheric conditions with SENS4ICE sensors and reference equipment and let ice form on the airframe with de-icing (pneumatic boots) active for safety reasons, after a certain time - preferably when all systems reliably indicated icing - the aircraft descended into warmer air and all ice accumulations were melted from the aircraft. This procedure was repeated until no icing conditions could be found anymore or the end of the flight test window was reached.

The data for the hereafter presented analysis were selected in order to have a reference across the SENS4ICE flight envelope including the icing flight test conditions. During the icing flights steady icing conditions representing either appendix C or appendix O conditions with a certain minimum length resulting in a noticeable degradation of aircraft aerodynamics were actively searched to fly in. Most data were recorded in steady horizontal flight, but there are also climb, descent, acceleration and deceleration segments included, see Figure 3. These segments build the base for the icing data used in the following longitudinal trim analysis. A summary of the data is given in Table 1, including an information about the encountered atmospheric characteristics [24]. Note that the data were gathered with different sample rates and resampled to 20 Hz for the flight data evaluations. As some instruments did only support low sample rates, e.g., 8 Hz, resampling to higher rates was not reasonable due to the lack of information content.

The data selection for steady conditions allows to make a clear discrimination between appendix C and appendix O conditions [14], but the effect of such icing on aircraft aerodynamics does of course change in its time related evolution

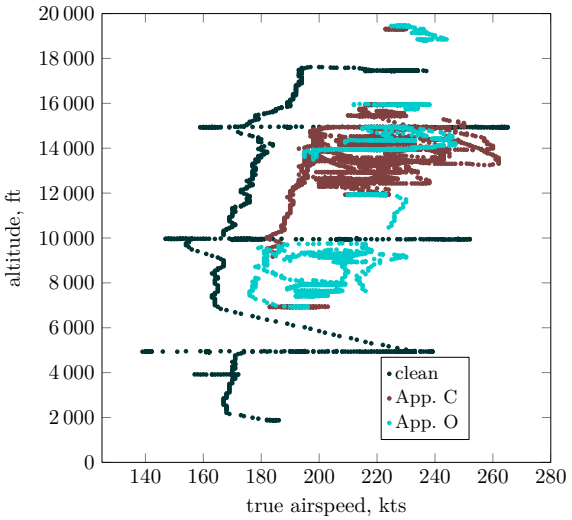

Fig. 3 Visualization of SENS4ICE European campaign flight data used for the longitudinal trim analysis: altitude vs. true airspeed for clean aircraft and different icing conditions.

from one encounter to another. Having natural icing during a flight test campaign, this needs to be accepted for the aircraft characteristics data evaluation. Hence, only a relatively general analysis of the effects of smaller and larger drops[‡] is possible. There is also no information about the specific ice formation on the aircraft for each data set available. Nevertheless, natural icing is a highly stochastic process and a more statistical analysis, as given below, is reasonable and possible with the available data.

Table 1 SENS4ICE European campaign flight data used for the longitudinal trim analysis; highest frequency of measurements obtained between -5 °C and -10 °C with mean MVD of 45 μm (see Ref. [24]).

data	size	number of segments	accumulated time	LWC
clean	62417	-	52.01 min	-
appendix C	200619	42	167.18 min	0.05 g/m^3 to 0.1 g/m^3
appendix O	119637	26	99.70 min	0.1 g/m^3 to 0.35 g/m^3

It is possible, that the data classified as appendix C or appendix O in this paper does also "contain effects of the other". In detail: if during one specific icing encounter in a cloud the droplet size changes significantly, there would be also a change of the classification, but of course, ice will form continuously on the airframe independent of the certification requirements. Hence, the effect could be mixed, especially, as there is no specific and sole appendix O encounter during a flight in icing conditions (at least in the presented flight test campaign). From a scientific point of view, it would be favorable to have a specific clustering in icing conditions and aerodynamic degradation, resulting in data sets with similar conditions and effects, built up solely by the related conditions. For natural icing flight tests, this would be challenging to obtain with a limited number of scientific flights. Within SENS4ICE during one month of testing with the thirteen flights 10 hours of different icing conditions were recorded. Trying to get more time in specific conditions would be almost impossible for practical reasons. For such test with specific aerodynamic effects on the test aircraft, flights with artificial icing are the only option. But then, the mapping of the natural icing effects including the stochastic ice built-up is not possible. For daily operations, the latter is the more important. Hence, the analysis of the data available with presented approach seems the most reasonable.

Figure 4 visualizes one encounter with steady appendix O conditions from the beginning (until 15:48 UTC) followed by an additional appendix C encounter until 15:56 UTC. The ice formation on the wing and empennage looks comparable in both cases. Visually it is difficult to discriminate between the ice accumulations for these short encounter times.

[‡]respectively appendix C and O conditions

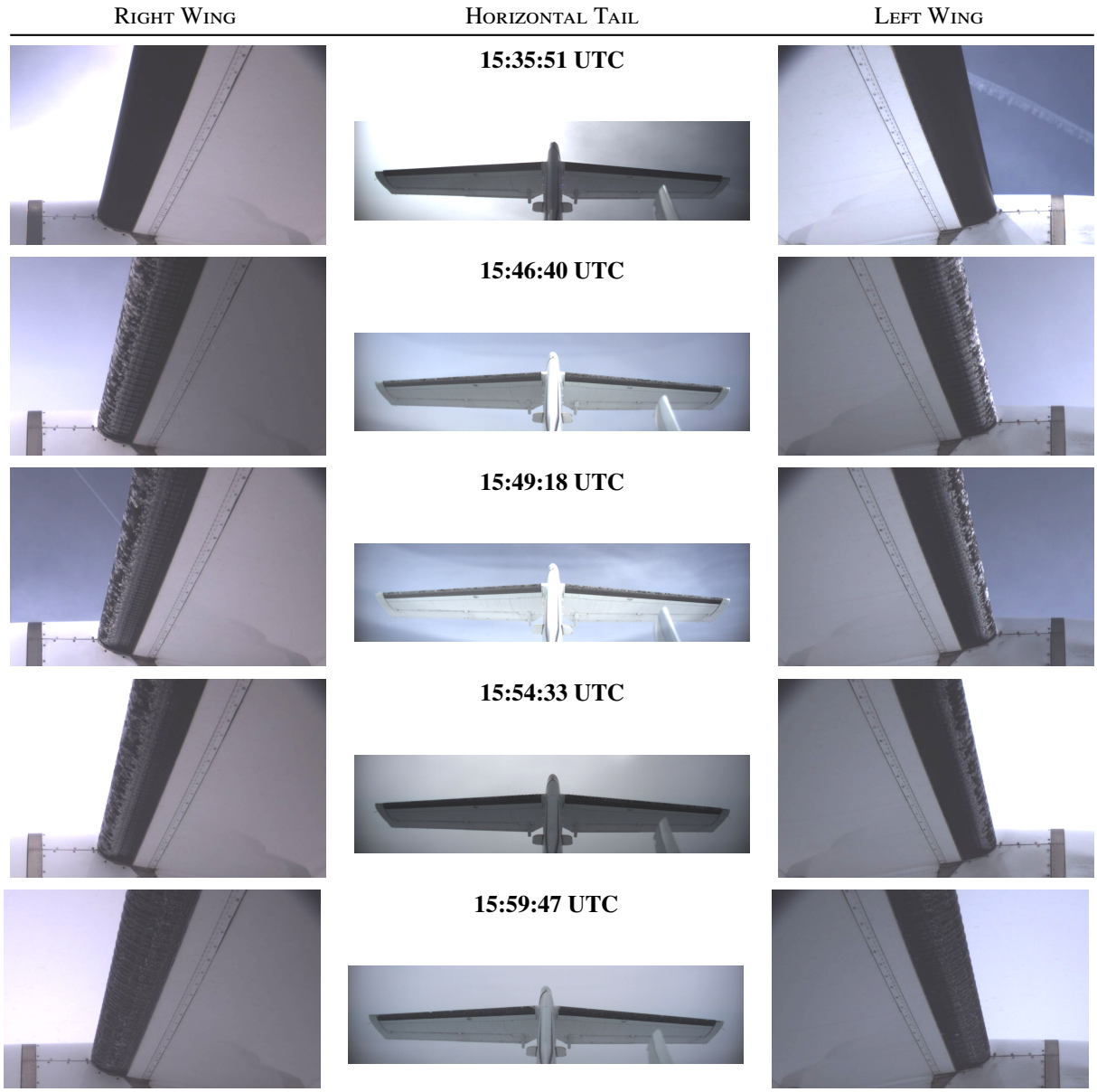

Fig. 4 Evolution of ice accretion on the airframe during icing encounter: camera views on left & right wing and horizontal tail for specific moments during flight (increased brightness and contrast); encounter time between 15:34 UTC and 16:03 UTC on 24th April, 2023; credit Safire / SENS4ICE project.

III. Flight Test Data Analysis

The flight data analysis is split into three sections: first the aircraft pitch trim analysis based on the measured aircraft data directly (c.f. section III.A). Second, the comparison of the lift and drag effects related to the different categories in the data (clean, appendix C and appendix O in section III.B). Third, the evaluation of the aircraft pitching moment coefficients calculated from flight data (c.f. section III.C).

A. Aircraft Pitch Trim Analysis

For aircraft longitudinal trim on the ATR 42, the elevator is used, without any variation of the horizontal tail plane. The aircraft's trim system is supported by trim tabs, which move the elevator into the desired direction. For flight mechanics, only the surface deflections producing an aerodynamic force (and moment around CG) are relevant. Hence the elevator deflection will be analyzed in this section, disregarding the trim tab used to trim the elevator in the desired position.

The SENS4ICE flight test data used for the analysis (see Fig. 3) shows that different altitudes and airspeeds for the different icing conditions and clean test flight do not perfectly match each other. Hence, a direct comparison of flight and icing conditions from the flight test campaign and the clean (ice-free) reference flight cannot be made. Furthermore, the icing conditions encountered do not automatically cause a specific aerodynamic degradation. The latter is subject to a stochastic atmospheric process and there is no direct correlation of icing conditions and ice formation on the airframe in natural icing flight test. In consequence, encountering specific icing conditions does not always lead to a specific need for a change in aircraft trim, which makes a direct comparison of data (flight and icing condition) even more difficult. Hence, the flight data will not be analyzed for specific altitudes or airspeed, but similar dynamic pressure, which is also more physically connected to the magnitude of the aerodynamic forces and moments. Figure 5 visualizes the elevator deflection vs. dynamic pressure. The clean flight data in this analysis covers a large variation of altitude and airspeed which directly results in a large variation of the required elevator deflection for the longitudinal aircraft trim. The icing conditions were encountered during the flight test within a safe icing flight test speed regime and at altitudes containing liquid water icing cloud layers. Hence, the dynamic pressure region for the icing data is much smaller than for the clean data. In addition, the data show a certain spread or variation of dynamic pressure for every elevator deflection or vice versa[§]. Although the aircraft was mainly flying with similar center of gravity[¶] there is a variation of total mass and CG between the flights and during the flight due to fuel consumption. Hence, different dynamics pressures flown could require different elevator deflections to trim the aircraft. Nevertheless, it is clearly visible, that the data follows a specific trend forming the elevator trim curve of the aircraft. Clean data as well as data from the icing flights follow this trend with no clear separation on a first glance.

To further reveal the dependency of elevator deflection required for trim, a regression with a nonlinear function $\eta = f(\overline{q})$ is used. The elevator deflection is approximated with:

$$\eta = P_{\eta,1} + P_{\eta,2} \cdot \sqrt{\overline{q}} + P_{\eta,3} \cdot \log(\overline{q}) \,. \tag{1}$$

Figure 6 gives an overview of the regression results (left side plot). In addition, the convex hulls including the flight data are plotted for each case. These envelopes ease the visualization of the overall data and allow a more direct data comparison than plotting each measurement. The three smaller plots on the right side of the figure show the results for each individual case: regression curve and convex hulls representing different percentiles of the data ($\mathcal{P}_{100}, \mathcal{P}_{99}, \mathcal{P}_{90}$). The hull curves contain the data with 90 % and 99 % variation related to the regression curve and 100 % of the data. It gets directly visible that the 90 % curve shows a much narrower band than the whole data set for each case. In addition, for the icing cases the resulting clean trim curve from the regression is given. The regression cost index (residual sum of squares) is printed bottom right. For clean and appendix O data, the results are well comparable in magnitude, but for the appendix C case it is three times higher. On the one hand, this indicates less representing regression results. But on the other hand, one has to keep in mind, that the appendix C data set is twice the size of the appendix O case and presumable contains much more variations of aerodynamic degradation resulting from icing than appendix O. It must be highlighted again, that the data is not clustered for similar aerodynamic icing effects but atmospheric conditions, which per definition introduces a larger variation in the results.

[§] note that the discrete layers in the of the elevator deflection shown in Fig. 5 results from the discrete measurement respectively recording during the SENS4ICE flight test with the standard systems of Safire ATR 42; no specific flight test instrumentation was available for obtaining a better resolution of the surface deflection.

[¶] all payload was fixed for the whole campaign, the variation in mass and CG results from different amounts of fuel on board and a different number of scientist and operators in the cabin for the flights.

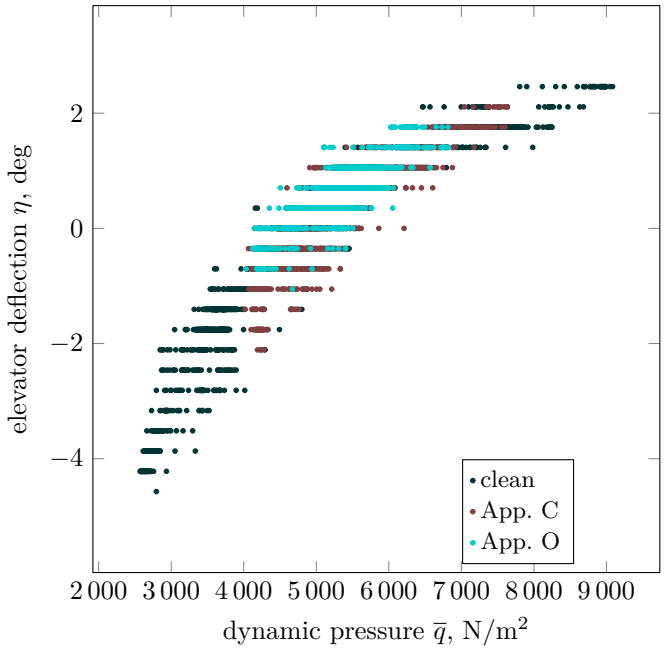

Fig. 5 Aircraft longitudinal trim for different icing cases: elevator deflection vs. dynamic pressure for the analyzed flight data; data from SENS4ICE European flight test campaign with Safire ATR 42-320.

The corresponding parameters of Equation (1) are given in Table 2. The results for the clean aircraft trim and the appendix C icing data are similar and do not reveal a directly noticeable change in the aircraft trim behavior. This matches the overall pilot reports from the flight test, in which the pilots did not state any abnormal aircraft behavior during the test campaign. But, the values of the regression function parameter indicate a (slightly) different curvature of the elevator trim curve, which is also visible in Fig. 6, especially for lower dynamic pressures. In contrast, the appendix O results show a different picture: The regression curve has less curvature and a shift to more positive (nose down) elevator deflections. This is also supported by the comparison of the parameters with the clean and appendix C case, with a much smaller logarithmic part in the result.

Table 2 Parameters of elevator regression function in Equation (1) for the different flight data sets from the SENS4ICE European flight test with Safire ATR 42-320.

(a) clean		**(b) appendix C**		**(c) appendix O**	
Parameter	Value	Parameter	Value	Parameter	Value
$P_{\eta,1}$	-117.503	$P_{\eta,1}$	-152.647	$P_{\eta,1}$	-21.465
$P_{\eta,2}$	-0.328	$P_{\eta,2}$	-0.459	$P_{\eta,2}$	0.061
$P_{\eta,3}$	16.550	$P_{\eta,3}$	21.764	$P_{\eta,3}$	2.057

To support the finding, that the curvature of regression results in case of icing represents the change in aircraft trim caused by icing, another regression of the icing data were calculated, but this time only shifting the clean trim curve with estimation of the parameter $P_{\eta,1}$, keeping the clean values for parameters $P_{\eta,2}, P_{\eta,3}$. The results are given in Figure 7 also including the regression cost index, which is worse in both icing cases compared to the "‘free"’ regression presented above. Nevertheless, the results clearly show more nose up tendency for the appendix O case, with less clear results for appendix C.

The trim data analysis show some effect of icing on the longitudinal pitch trim and required elevator deflection, but the recorded flight data itself does not reveal any conclusive facts.

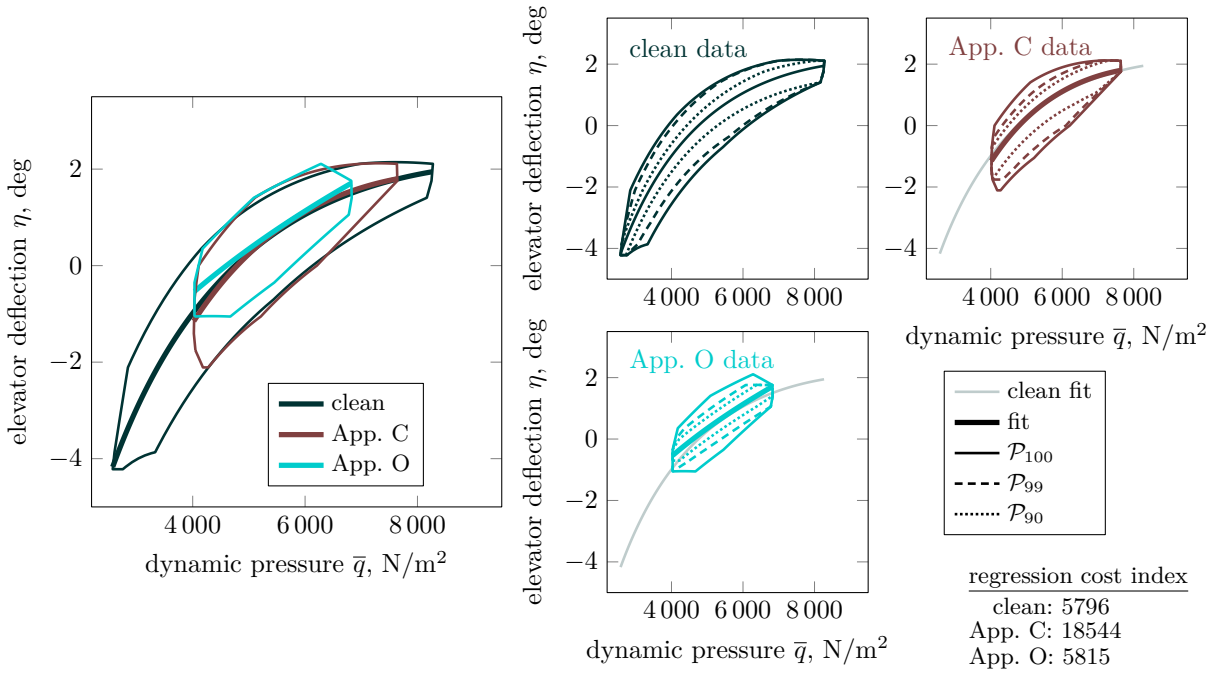

Fig. 6 Detailed visualization of aircraft longitudinal trim for different icing cases: elevator deflection vs. dynamic pressure for the analyzed flight data; regression curves and convex hulls; data from SENS4ICE European flight test campaign with Safire ATR 42-320.

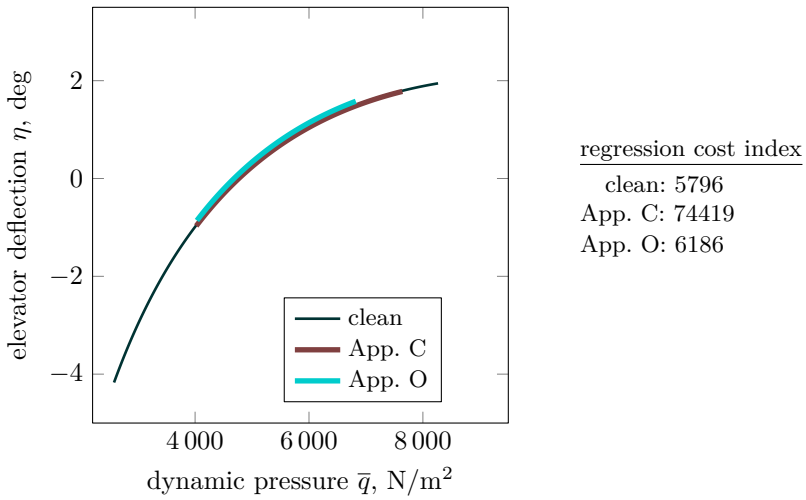

Fig. 7 Visualization of aircraft longitudinal trim regression curves for different icing cases with sole linear shift of clean curve: elevator deflection vs. dynamic pressure for the analyzed flight data; data from SENS4ICE European flight test campaign with Safire ATR 42-320.

B. Lift and Drag Evaluation

The next step of the analysis is the lift and drag evaluation. The aerodynamic forces are directly computed from the measured flight data and the available engine thrust model provided by ATR for the SENS4ICE flight data campaign.

The propeller axis are approximately aligned with the aircraft's body longitudinal axis, which leads to the following assumption for the further calculations related to the total engine thrust vector of both engines/propellers:

$$T_{\mathrm{x}} \approx T_{\mathrm{total}} \tag{2}$$

The longitudinal aerodynamic force coefficient in body axis with respect to the center of gravity results from

$$C_{X,\mathrm{meas,CG}} = \frac{m_{\mathrm{AC}} \cdot a_{\mathrm{x,CG}} - T_{\mathrm{x}}}{\overline{q} \cdot S_{\mathrm{Wing}}}\,, \tag{3}$$

and the vertical aerodynamic force coefficient is approximated by

$$C_{Z,\mathrm{meas,CG}} \approx \frac{m_{\mathrm{AC}} \cdot a_{\mathrm{z,CG}}}{\overline{q} \cdot S_{\mathrm{Wing}}} \tag{4}$$

neglecting presumably small forces resulting from the propellers in vertical direction.

Transformation of these coefficients in the experimental coordinate system with the angle of attack results in the aircraft's total drag coefficient

$$C_{D,\mathrm{meas,CG}} = -C_{X,\mathrm{meas,CG}} \cdot \cos(\alpha) - C_{Z,\mathrm{meas,CG}} \cdot \sin(\alpha) \tag{5}$$

and total lift coefficient

$$C_{L,\mathrm{meas,CG}} = \quad C_{X,\mathrm{meas,CG}} \cdot \sin(\alpha) - C_{Z,\mathrm{meas,CG}} \cdot \cos(\alpha)\,. \tag{6}$$

A standard approach for a lift coefficient regression model is the following linear formulation with the angle of attack

$$C_L = C_{L0} + C_{L\alpha} \cdot \alpha \tag{7}$$

which is used to fit the calculated lift coefficients from Equation (6). Fig. 8 contains the regression results for the different icing cases and clean data on the left side. There is a slight reduction in lift slope for icing revealed meeting the expectations. But there is no significant change of lift behavior during the flight test campaign, which in line with the pilot reports from the campaign flights. On the right side of the figure, the three different smaller plots contain the individual regression curve results for each case[‖] including the convex hulls enveloping 99 % ($\mathcal{P}_{99}$) and 100 % ($\mathcal{P}_{100}$) of the corresponding data. There is a noticeable stronger variation in case of appendix O (between $\mathcal{P}_{99}$ and $\mathcal{P}_{100}$), which source could not determined directly. Nevertheless, the $\mathcal{P}_{99}$ curve show that most of the data is well represented by the regression curve.

The drag coefficient function also follows the standard quadratic polar formulation

$$C_D = C_{D0} + k_2 \cdot C_L^2\,. \tag{8}$$

Note that for the regression the data calculated from measurements for the lift coefficient are used in Equation (6) and not the model fit calculated with Equation (7). The latter could also be used, but it might change the results removing some variation present in the data (as given in Fig. 8).

Figure 9 contains the drag coefficient calculation and regression results as drag polars for the clean and icing cases on the left. On the right, the results for each case are presented including the convex hulls enveloping 90 % ($\mathcal{P}_{90}$) , 99 % ($\mathcal{P}_{99}$) and 100 % ($\mathcal{P}_{100}$) of the corresponding data.

The observed drag coefficient variation in all cases for 99 % of the data (and above) is noticeably high, but was already observed during the SENS4ICE post flight data analysis and evolution. It might be a direct result from the data measurements with different sensor accuracy, but could also result from uncertainties in the aircraft weight and balance prediction or the used simplified engine/propeller thrust model. Nevertheless, the regression results can predict the underlying drag characteristics of the aircraft in all cases very well. For icing, there is a noticeable drag increase in both cases, which was expectable and also revealed by the results of the SENS4ICE developed IID (c.f. Refs. [10–12]).

[‖] evaluated for the whole angle of attack region present in the data

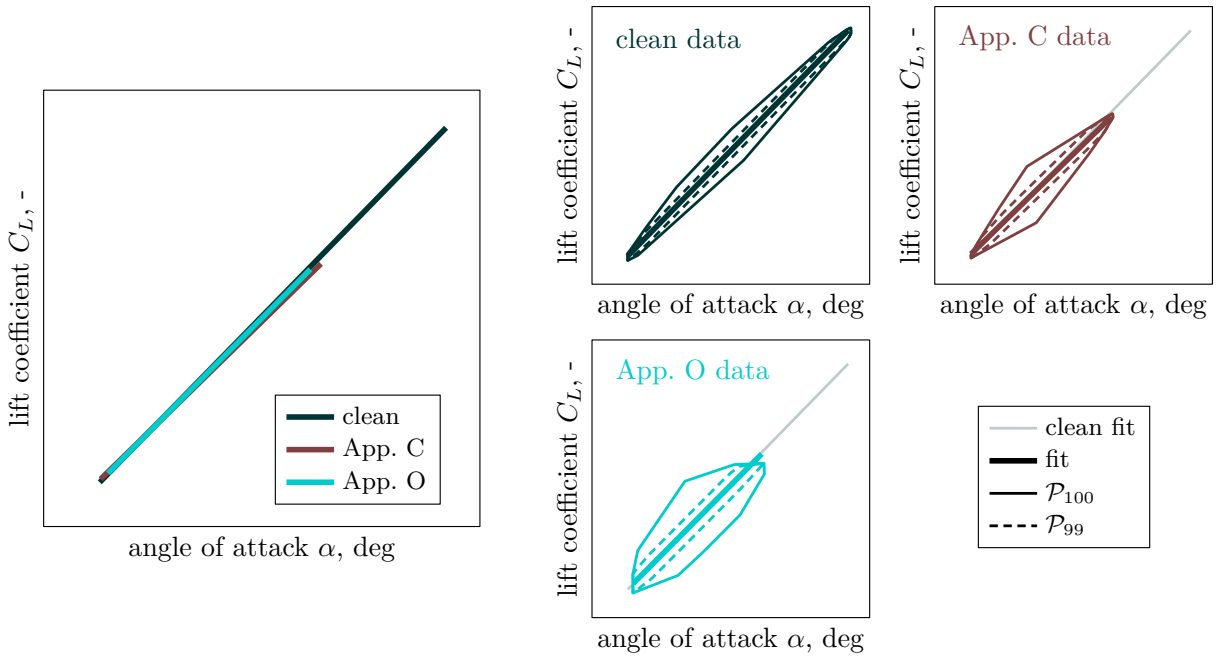

Fig. 8 Detailed visualization of aircraft lift coefficient for different icing cases: lift coefficient vs. angle of attack for the analyzed flight data; regression curves and convex hulls; data from SENS4ICE European flight test campaign with Safire ATR 42-320.

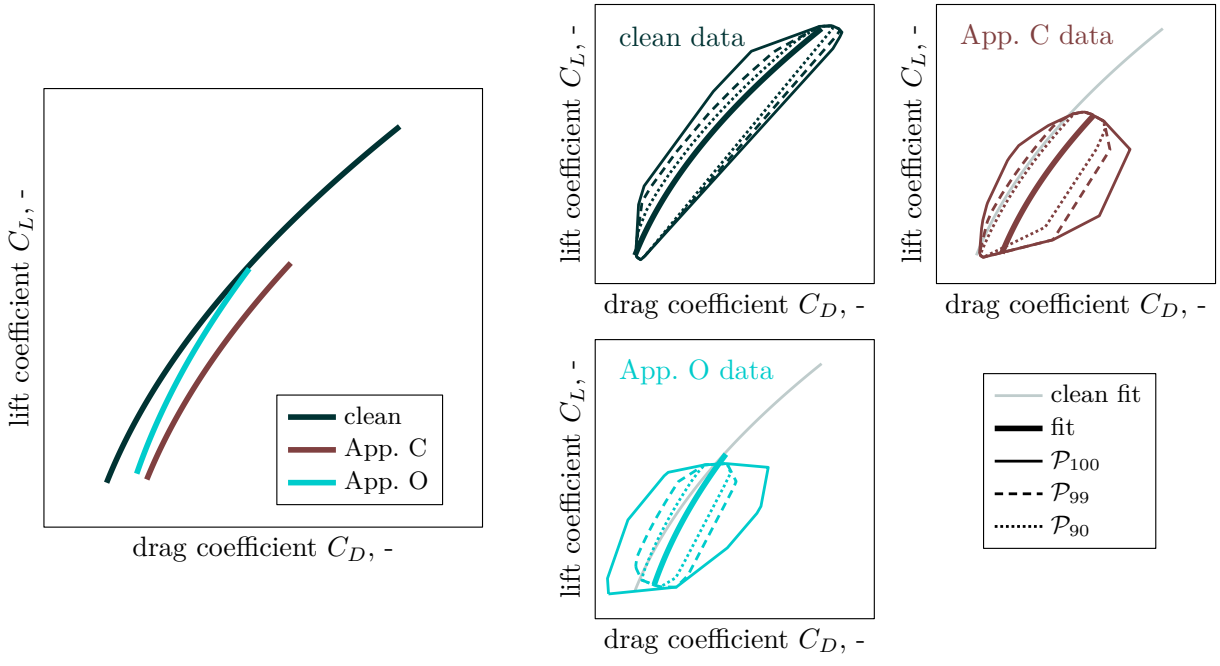

Fig. 9 Detailed visualization of aircraft drag coefficient for different icing cases: lift coefficient vs. drag coefficient for the analyzed flight data; regression curves and convex hulls; data from SENS4ICE European flight test campaign with Safire ATR 42-320.

C. Pitching Moment Evaluation

Finally, the pitching moment coefficient calculated from the flight test data is evaluated. The total moment is composed from a dynamic influence, the engine moment and the aerodynamic pitching moment. In the present case the engine moment is approximated by the engine forces and the lever arm with respect to CG. It can be calculated as follows:

$$M_{T_{\text{total}}} \approx (z_{\text{CG}} - z_{\text{RP}}) \cdot T_{\text{x}} \mathrel{\widehat{=}} (z_{\text{CG}} - z_{\text{RP}}) \cdot T_{\text{total}} \tag{9}$$

With a known $M_{T_{\text{total}}}$ the resulting aerodynamic pitching moment (at CG) is:

$$M_{\text{aero,CG}} = I_{\text{yy}} \cdot \dot{q} + \left(I_{\text{xx}} - I_{\text{yy}}\right) \cdot p \cdot r + I_{\text{xz}} \cdot \left(p^2 - r^2\right) - M_{T_{\text{total}}}. \tag{10}$$

The pitching moment coefficient at CG can be defined as

$$C_{m,\text{aero,CG}} \mathrel{\widehat{=}} \frac{M_{\text{aero,CG}}}{\overline{q} \cdot S_{\text{Wing}} \cdot \bar{c}}\,. \tag{11}$$

A linear regression for the aerodynamic pitching moment (see Equation (12)) with the angle of attack is used to further reveal the changes related to icing.

$$C_m = C_{m0} + C_{m\alpha} \cdot \alpha\,. \tag{12}$$

An overview of the resulting coefficients is given in Table 3.

Table 3 Parameters of pitch moment regression function in Equation (12) for the different flight data sets from the SENS4ICE European flight test with Safire ATR 42-320; relative change compared to base (clean) configuration.

(a) appendix C

Parameter	Value
ΔC_{m0}	35.4 %
$\Delta C_{m\alpha}$	-9.8 %

(b) appendix O

Parameter	Value
ΔC_{m0}	62.2 %
$\Delta C_{m\alpha}$	-23.2 %

In Fig. 10 the pitch moment coefficient curves versus angle of attack after regression for the clean aircraft and icing cases are presented on the left side. On the right side, the convex hulls enveloping all data, the 99 % and 90 % percentiles are plotted. Similar to the lift and drag curves in Figs. 8 and 9 the data distribution shows a strong variation within the last 1 % of data, already discussed above.

In case of icing, there are two major effects visible in the data, which are comparable to results in Ref. [19] and Ref [20] for NASA's DHC-6 Twin Otter, but in contrast to the expectations in Fig. 2b:

1) the aircraft shows a reduced pitching moment respectively a more nose up tendency for the lower angles of attack;
2) the pitching moment negative slope is increased (see also Table 3) respectively steeper negative with the angle of attack, leading to a more static steady behavior.

The effect on the pitching moment can also be deduced from the present change of aerodynamic forces. In case of ice accretion on the airframe the aircraft drag increases, as shown in Fig. 9, which will directly lead to a change in trim characteristics. For constant speed, the increase in drag (in body fixed longitudinal direction) will be compensated with an increase of propeller thrust, and as both forces are not in the same vertical distance to the center of gravity, there will be a resulting pitch up moment present to be compensated by the elevator. This is visualized in Fig. 11.

The resulting additional pitch moment from thrust increase to compensate the increased drag is given by

$$\Delta M = \Delta F_{D,x} \cdot \Delta z_{\text{CG,RP}} - \Delta T_{\text{total}} \cdot \Delta z_{\text{CG,prop}} \tag{13}$$

with

$$\Delta z = \Delta z_{\text{CG,RP}} - \Delta z_{\text{CG,prop}} \tag{14}$$

and can be approximated with the assumption that $\|F_{D,x}\| \approx \|\Delta T_{\text{total}}\|$

$$\Delta M \approx \Delta F_{D,x} \cdot \Delta z\,. \tag{15}$$

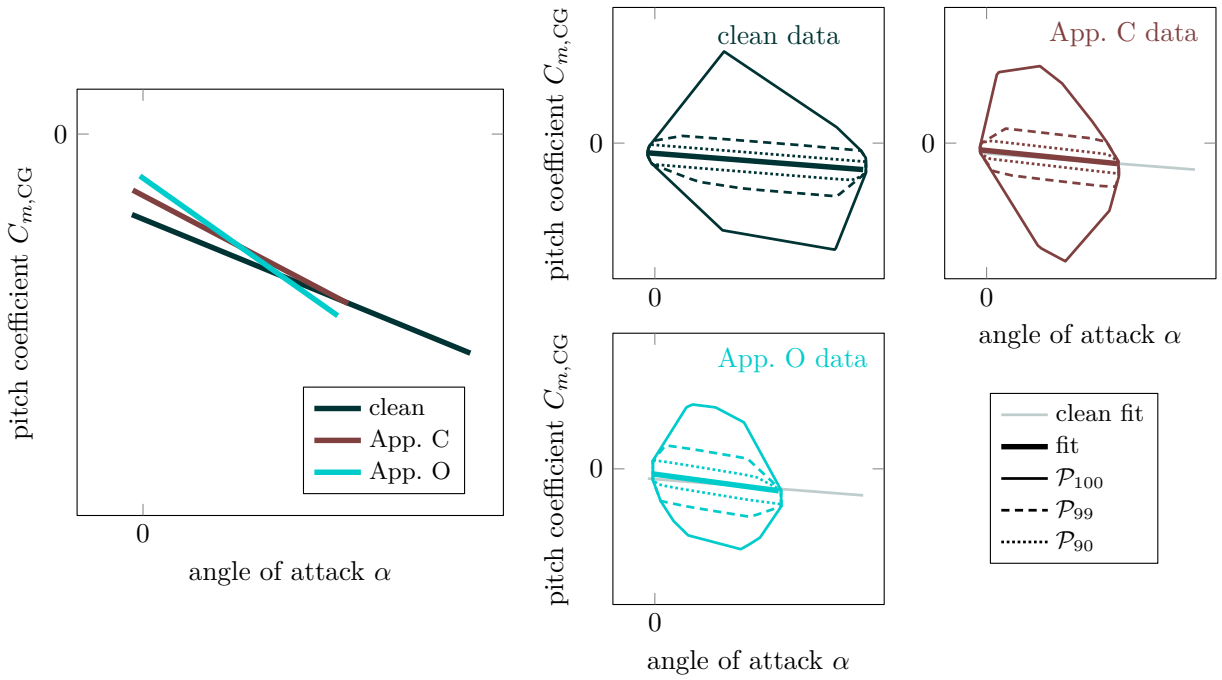

Fig. 10 Detailed visualization of aircraft pitch coefficient for different icing cases: pitch moment coefficient vs. angle of attack for the analyzed flight data; regression curves and convex hulls; data from SENS4ICE European flight test campaign with Safire ATR 42-320.

This directly shows, that the larger the drag increase caused by icing, the larger the nose up pitch tendency. For the present case of the SENS4ICE European flight test campaign with the Safire ATR 42, the main effect of icing on longitudinal trim seems to be related to the change of aerodynamic forces. Nevertheless, there might be also a change of the wing's aerodynamic pitch moment and neutral point and/or the stabilizer aerodynamics reducing its effect, but this cannot be further determined with the data recordings available. But it seems more likely based on the given evaluation that the change in drag (and thrust) are the main cause of longitudinal trim effects.

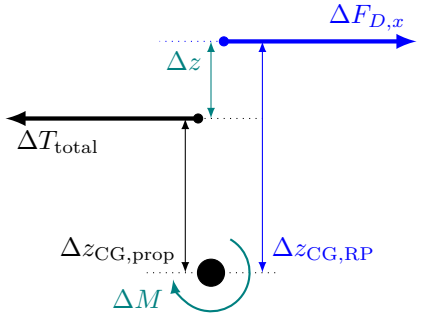

Fig. 11 Schematic visualization of aircraft center of gravity and force application points.

Exploitation and limitation of evaluation results

It is important to state, that the regression curves provided above should not be used to model icing in an aerodynamic model formulation. The correspondence between aerodynamic effects and flight data recordings is not bijective. It is clear, that the regression done to obtain the trend curves on the pitching moment combine the effects of different icing encounters and deliver an assessment of the difference in icing effects on the aerodynamics, especially the aircraft pitching moment. But it is not the case, that specific icing conditions will "always" cause the same effect, as the effects are mainly dependent on the specific shapes as already mentioned. Nevertheless, the evaluation allows drawing one conclusion on the general change on aerodynamics for the longitudinal trim, namely the overall pitch up / nose up tendency.

IV. Conclusion

In this paper an analysis of the aircraft longitudinal trim for different icing conditions is presented. Based on data from the SENS4ICE European flight test campaign in 2023 with the Safire ATR 42 research aircraft, the change in trim state and the overall aircraft pitching moment due to App. C and App. O icing are evaluated. In all cases, either individual encounters or generalized for the certification envelopes (App. C or App. O), the aircraft showed in general a nose up pitch tendency, especially for lower angles of attack. This in-line with results from NASA for the Twin Otter in icing, but in contrast to some expectations from literature. The results provided are related to potential natural icing accumulation on all unprotected surfaces at the aircraft and also the protected surfaces between the de-icing cycles of the mechanical/pneumatic protection system. In addition to the inter-cycle ice, also residual ice might be present. Moreover, the ice shapes are not fully monitored and are by high chance not similar between the encounters. Hence, the real flight data from natural icing is not homogeneous in terms of icing and ice shapes (also including varying conditions within the certification envelopes used for clustering) and the resulting aerodynamic effects. But nevertheless, the analysis of the required elevator use for trimming the aircraft showed only a minor influence on the aircraft trim state and hence the flight behavior during the icing encounters noticeable by the pilots. On the opposite, the significant increase of drag directly requires a higher thrust setting to maintain the flight conditions, which is a more significant indicator of aircraft degradation for the pilots and more relevant to the flight operations.

Funding Information

The "SENSors and certifiable hybrid architectures for safer aviation in ICing Environment" (SENS4ICE) project has received funding from the European Union's Horizon 2020 research and innovation programme under grant agreement N° 824253.

Acknowledgments

The authors want to specially honor the work of Bruno Thillays and Annagrazia Orazzo from SAFRAN Aerosystems on developing the HIDS implementation for the SENS4ICE flight tests.

The Airborne data was obtained using the aircraft managed by Safire, the French facility for airborne research, an infrastructure of the French National Center for Scientific Research (CNRS), Météo-France and the French National Center for Space Studies (CNES). Distributed data are processed by SAFIRE. The author wants to specially thank the SENS4ICE European campaign flight test team for its structured and professional work to conduct the flight tests even on very short notice according to the weather forecasts. A special thank goes to Tetyana Jiang (Safire) for the support with the flight test instrumentation, flight data and in-flight camera footage, and Jean-Philippe Desbios (Safire) for the campaign coordination.

References

[1] Green, S. D., "A Study of U. S. Inflight Icing Accidents and Incidents, 1978 to 2002," 44th AIAA Aerospace Sciences Meeting and Exhibit, American Institute of Aeronautics and Astronautics, Inc. (AIAA), Reno, Nevada, USA, 2006. https://doi.org/10.2514/6.2006-82.

[2] Green, S. D., "The Icemaster Database and an Analysis of Aircraft Aerodynamic Icing Accidents and Incidents," Technical Report DOT/FAA/TC-14/44, R1, Federal Aviation Administration, Atlantic City, NJ, USA, Oct. 2015.

[3] Anon., *Final Report (BFU 5X011-0/98)*, German Federal Bureau of Aircraft Accident Investigation, Braunschweig, Germany, April 2001.

[4] Anon., *Aircraft Accident Report (NTSB/AAR-96/01, DCA95MA001), Safety Board Report*, National Transportation Safety Board (NTSB), Washington, DC, USA, July 9th 1996.

[5] Deiler, C., and Fezans, N., "Performance-Based Ice Detection Methodology," *Journal of Aircraft*, Vol. 57, No. 2, 2020, pp. 209–223. https://doi.org/10.2514/1.C034828.

[6] Deiler, C., and Sachs, F., "Design and Testing of an Indirect Ice Detection Methodology," SAE International Conference on Icing of Aircraft, Engines, and Structures, SAE International, Paper 2023-01-1493, Vienna, Austria, 2023. https://doi.org/10.4271/2023-01-1493.

[7] Schwarz, C. W., "The SENS4ICE EU project – SENSors and certifiable hybrid architectures for safer aviation in ICing Environment – Project Overview and Initial Results," 33th Congress of the International Council of the Aeronautical Sciences (ICAS), Stockholm, Sweden, 2022. URL https://icas.org/ICAS_ARCHIVE/ICAS2020/data/papers/ICAS2022_0794_paper.pdf.

[8] Schwarz, C. W., "SENS4ICE EU Project Preliminary Results," SAE International Conference on Icing of Aircraft, Engines, and Structures, SAE International, Paper 2023-01-1496, Vienna, Austria, 2023. https://doi.org/10.4271/2023-01-1493.

[9] Schwarz, C. W., Deiler, C., Lucke, J., Jurkat-Witschas, T., Orazzo, A., and Thillays, B., "SENS4ICE EU Project Hybrid Ice Detection Architectures Demonstration Results," 34th Congress of the International Council of the Aeronautical Sciences (ICAS), Florence, Italy, 2024. URL https://www.icas.org/icas_archive/icas2024/data/papers/icas2024_0178_paper.pdf.

[10] Deiler, C., "Performance-Based Ice Detection First Results from SENS4ICE European Flight Test Campaign," AIAA Scitech Forum, American Institute of Aeronautics and Astronautics, Inc. (AIAA), Orlando, Florida, USA, 2024. https://doi.org/10.2514/6.2024-2817.

[11] Deiler, C., "Flight Test Results for Performance-Based Ice Detection," 34th Congress of the International Council of the Aeronautical Sciences (ICAS), Florence, Italy, 2024. URL https://www.icas.org/icas_archive/icas2024/data/papers/icas2024_0046_paper.pdf.

[12] Deiler, C., "Testing of an Indirect Ice Detection Methodology in the Horizon2020 Project SENS4ICE," *CEAS Aeronautical Journal*, 2024. https://doi.org/10.1007/s13272-024-00783-1.

[13] Deiler, C., and Fezans, N., "Method and assistance system for detecting a degradation of flight performance," , 2017. Patent Numbers: US11401044B2, EP3479181B1, WO2018002148A1, FR3053460B1, CA3029467A1, ES2919573T3.

[14] Jurkat-Witschas, T., Lucke, J., Schwarz, C. W., Deiler, C., Sachs, F., Kirschler, S., Menekay, D., Voigt, C., Bernstein, B., Jaron, O., Kalinka, F., Zollo, A., Lilie, L., Mayer, J., Page, C., Vié, B., Bourdon, A., Pereira Lima, R., and Vieira, L., "Overview of Cloud Microphysical Measurements During the SENS4ICE Airborne Test Campaigns: Contrasting Icing Frequencies from Climatological Data to First Results from Airborne Observations," SAE International Conference on Icing of Aircraft, Engines, and Structures, SAE International, Paper 2023-01-1491, Vienna, Austria, 2023. https://doi.org/10.4271/2023-01-1491.

[15] Sachs, F., Schwarz, C. W., and Deiler, C., "Flight Testing the Indirect Ice Detection System in the Horizon 2020 Project SENS4ICE," AIAA Aviation Forum and ASCEND, American Institute of Aeronautics and Astronautics, Inc., Las Vegas, Nevada, USA, 2024. https://doi.org/10.2514/6.2024-3524.

[16] Anon., "Ice Accretion Simulation," AGARD Advisory Report 344, Advisory Group for Aerospace Research & Development (AGARD) - Fluid Dynamics Panel Working Group 20, North Atlantic Treaty Organization (NATO), Neuilly-Sur-Seine, France, December 1997.

[17] Bragg, M. B., "Aircraft Aerodynamic Effects Due To Large Droplet Ice Accretions," 34th AIAA Aerospace Sciences Meeting and Exhibit, American Institute of Aeronautics and Astronautics, Inc. (AIAA), AIAA 96-0932, Reno, Nevada, USA, 1996. https://doi.org/10.2514/6.1996-932.

[18] Bragg, M. B., Perkins, W. R., Sarter, N. B., Başar, T., Voulgaris, P. G., Gurbacki, H. M., Melody, J. W., and McCray, S. A., "An Interdisciplinary Approach to Inflight Aircraft Icing Safety," 36th AIAA Aerospace Sciences Meeting and Exhibit, American Institute of Aeronautics and Astronautics, Inc. (AIAA), Reno, Nevada, USA, 1998. https://doi.org/10.2514/6.1998-95.

[19] Ranaudo, R. J., Mikkelsen, K. L., McKnight, R. C., Ide, R. F., Reehorst, A. L., Jordan, J. L., Schinstock, W. C., and Platz, S. J., "The Measurement of Aircraft Performance and Stability and Control After Flight Through Natural ICing Conditions," American Institute of Aeronautics and Astronautics, Inc. (AIAA), Las Vegas, Nevada, USA, 1986. https://doi.org/10.2514/6.2002-4605.

[20] Ratvasky, T. P., and Ranuado, R. J., "Icing Effects on Aircraft Stability and Control Determined from Flight Data. Preliminary Results," 31st AIAA Aerospace Sciences Meeting and Exhibit, American Institute of Aeronautics and Astronautics, Inc. (AIAA), Reno, Nevada, USA, 1993. https://doi.org/10.2514/6.1993-398.

[21] Broeren, A. P., Whalen, E. A., Busch, G. T., and Bragg, M. B., "Aerodynamic Simulation of Runback Ice Accretion," *Journal of Aircraft*, Vol. 47, No. 3, 2010, pp. 924–939. https://doi.org/10.2514/1.46475.

[22] Lee, S., Barnhart, B. P., and Ratvasky, T. P., "Dynamic Wind-Tunnel Testing of a Sub-Scale Iced S-3B Viking," AIAA Atmospheric and Space Environments Conference, American Institute of Aeronautics and Astronautics, Inc. (AIAA), Toronto, Ontario, Canada, 2010. https://doi.org/10.2514/6.2010-7986.

[23] Deiler, C., "Performance-Based Ice Detection First Results from SENS4ICE European Flight Test Campaign," AIAA Scitech Forum, American Institute of Aeronautics and Astronautics, Inc. (AIAA), Orlando, Florida, USA, 2024. https://doi.org/10.2514/6.2024-2817.

[24] Lucke, J., Zollo, A. L., Bernstein, B., and Jurkat-Witschas, T., "Final report on airborne demonstration and atmospheric characterisation," SENS4ICE Deliverable D4.3, DLR, February 6th 2024. URL https://ec.europa.eu/research/participants/documents/downloadPublic?documentIds=080166e50877b390&appId=PPGMS.